Electrochemical and Solid-State Letters, **9** (11) A499-A503 (2006)
1099-0062/2006/9(11)/A499/5/$20.00 © The Electrochemical Society

In Situ Imaging of Liquid Water and Ice Formation in an Operating PEFC during Cold Start

Shanhai Ge and Chao-Yang Wang[*,z]

Electrochemical Engine Center and Department of Mechanical and Nuclear Engineering, The Pennsylvania State University, University Park, Pennsylvania 16802, USA

A transparent polymer-electrolyte fuel cell (PEFC) was developed to study liquid water and ice formation during startup from subzero temperatures. A silver mesh was used as the cathode gas diffusion layer to allow direct observation of phase transition and water transport on the surface of the catalyst layer (CL). It was found that at a current density of 0.02 A/cm^2 and startup temperature of −5°C, water exists in the cathode CL in solid and gas phases. At startup temperatures higher than −3°C, however, water droplets are found on the CL surface and the cold-start operation is significantly prolonged. It is therefore suggested that the freezing-point depression of water in the cathode CL is no greater than 2°C and plays a negligible role in cold-start theory and practice.
 [DOI: 10.1149/1.2337860]

Manuscript submitted May 25, 2006; revised manuscript received July 4, 2006. Available electronically August 29, 2006.

Cold-start capability and survivability of polymer electrolyte fuel cells (PEFCs) in a subzero environment remain a major challenge for automotive applications. Its fundamental mechanisms are not fully determined, but it is recognized that product water becomes ice or frost upon startup when the PEFC internal temperature is below the freezing point of water. If the local pore volume of the cathode catalyst layer (CL) is insufficient to contain all of the accumulated water before the cell operating temperature rises above freezing, solid water may plug the catalyst layer and stop the electrochemical reaction by starving the reagent gases. In addition, ice formation may result in serious damage to the structure of a membrane electrode assembly (MEA).

In spite of the importance of PEFC cold-start capability and associated MEA durability, very few studies in the literature have focused on PEFC startup dynamics, freeze/thaw cycling,[1-8] and characterization of Nafion membrane at temperatures below 0°C.[9-11] Wilson et al.[1] showed that cell operation at −10°C does not adversely impact the MEA integrity even with high water content. Cho et al.[2] showed performance degradation in a cell without gas purge, i.e., containing a membrane with high water content, after freeze/thaw cycling between −10 and 80°C. In particular, the electrochemically active area decreases and the membrane resistance rises. Their later study demonstrated that if the cell is purged with dry gas for 20 min, almost no performance degradation or increase in membrane resistance can be observed after the freeze/thaw cycling.[3] McDonald et al.[4] also observed that the temperature dependence of the proton conductivity of Nafion 112 membrane does not change in slope, indicating that no phase transition of water within the membrane and no CL degradation occur, for dry MEA subject to freeze/thaw cycling between −40 and 80°C. St-Pierre et al.[5] found that if a cell was purged with dry gas at 85°C (hot purge), progressive performance losses were observed, attributable to mass transport after freeze/thaw cycling, while in a cell purged with dry gas at 20°C (cool purge), performance losses were not observed.

Obviously, self-startup from a subfreezing temperature without an external heat source is advantageous for PEFC engines. Kagami et al.[6] pointed out that it would be possible to sustain operation of a single cell at a subfreezing temperature by balancing the amount of product water with water removed from the cell. However, because the saturated vapor pressure of water at temperatures below 0°C is very low, the flow rates of reactant gases would have to be extremely high in order to adequately remove water produced by the oxygen reduction reaction (ORR). This large quantity of gas would simultaneously take away the heat generated by the cell, thereby rendering the warm-up period of a fuel cell stack impractically long. Indeed, the simulation results of Hishinuma et al.[7] showed that cell start up is difficult from temperatures below −5°C using large gas flow rates to remove product water. Most recently, Oszcipok et al.[8] demonstrated that in a cell purged with dry nitrogen prior to freezing, cumulated charge density can reach 70 C/cm^2 during a potentiostatic cold start from −10°C. Ice formation in the cathode CL was found to result in both a current density reduction of ~5.4% (at 0.45 V) for each cold start and a decrease in the electrochemically active surface area of the cathode CL. It was explained that the water contents in the membrane and ionomers of the CL are lowered by the purge process prior to cold start, which extends the cold-start operational time. When cell temperature becomes higher than 0°C, a fuel cell can operate stably in spite of environmental temperatures of −10 or −20°C,[12,13] or even in the Antarctic.[14]

We present here a first visual study of ice and liquid water formation on the cathode CL surface in an operating fuel cell during cold start from various ambient temperatures. The objective is to help elucidate the fundamental physics of ice formation during PEFC cold start, and particularly to address the degree of the freezing-point depression of water within micropores of the cathode CL.

Experimental

A catalyst-coated membrane (CCM) based on an 18 μm thick Gore–Select membrane was sandwiched between poly(tetrafluoroethylene) (PTFE)-proofed carbon paper with microporous layer (GDL 20BB, SGL) and silver mesh (McMaster-Carr) as the anode and cathode gas diffusion layers (GDL), respectively. The Pt loadings in the anode and cathode catalyst layers are both 0.4 mg/cm^2. The active area of the electrode is 5 cm^2. Two gold-plated stainless steel current collector sheets were machined to form a single-pass serpentine flowfield with channels 1 mm wide and 0.5 mm deep. A transparent polycarbonate plate was placed outside of the cathode current collector sheet to provide optical access. The polycarbonate plate and anode current collector sheet were clamped by two stainless steel end plates. A window was cut in the cathode end plate. Figure 1 shows a diagram of the transparent cell structure and an image of the normal view from the cathode side. The width of each land in the flowfield is 1 mm. The open area and wire diameter of the silver mesh are 0.38 × 0.38 mm and 0.24 mm, respectively. The open area of the silver mesh offers direct observation of water behavior on the CL surface during cell operation.

The cell was connected to a fully computer-controlled fuel cell test station (Arbin Instruments), which regulates the current density and the operating conditions. The pressures of the anode and the cathode were both kept at 1 atm (absolute). The end plate temperature was controlled using a built-in heat exchanger with circulating antifreeze coolant. The cell was preconditioned by operating it with fully humidified hydrogen and air at low stoichiometric ratios and at

* Electrochemical Society Active Member.
[z] E-mail: cxw31@psu.edu

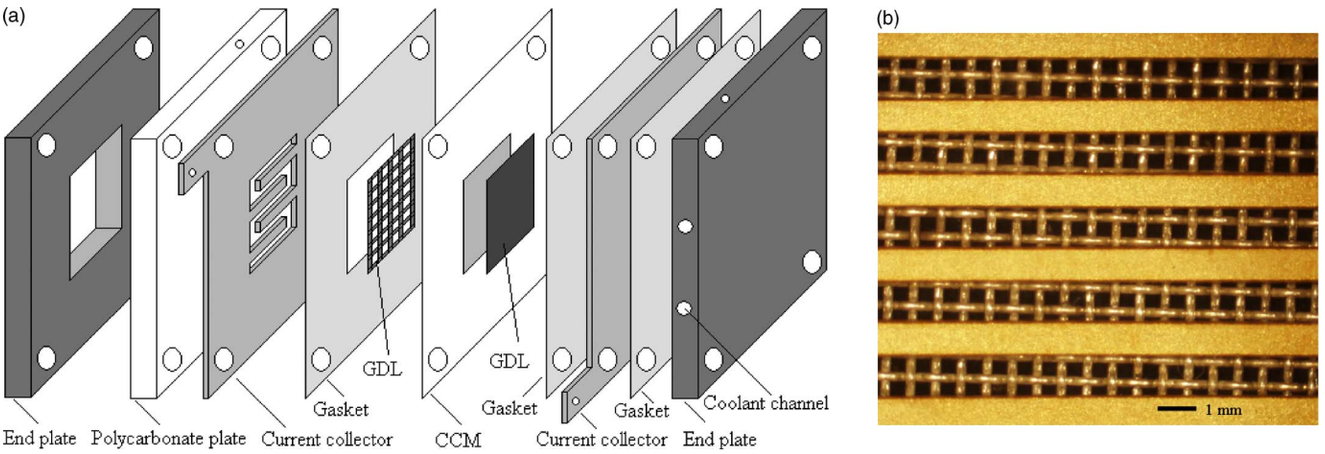

Figure 1. (Color online) (a) Schematic of the cell structure and (b) picture of the serpentine flowfield with the flow channel of 1 mm wide and 0.5 mm deep. The opening area and wire diameter of the silver mesh are 0.38 × 0.38 mm^2 and 0.24 mm, respectively.

80°C for 6 h. Before cooling down and starting up the cell at a subfreezing temperature, both anode and cathode were purged with dry nitrogen at flow rates of 400 and 900 mL/min, respectively. The duration of purge was 2 min in all experiments. During gas purge, the temperatures of the cell and inlet gases were kept at 55°C. After purging the cell, the gas inlets and outlets were shut off and the coolant was circulated through the end plate to lower the cell temperature to a prescribed startup temperature. When starting up the cell at the subfreezing temperature, dry hydrogen and air were fed to the cell at a flow rate of 20 mL/min (or 1.487×10^{-5} mol/s) under standard temperature and pressure (stoichiometric ratios: $\xi_{H2} = 28.7$, $\xi_{air} = 12.1$ at $i = 0.02$ A/cm^2). The current density was kept constant at 0.02 A/cm^2 during each startup and the cell potential was recorded. When cell potential dropped to 0.1 V, cold-start operation was cut off. Cold-start tests along with in situ imaging were conducted at −5, −3, and −1°C, respectively.

A digital camera (Olympus DP 70) combined with a zoom lens (Navitar) were used to record micrographs using external halogen illumination. The imaging and camera systems used can resolve features down to 1 μm. Other details of the visualization setup can be found in our previous work.[15,16] High-frequency resistance (HFR) measurements (Tsuruga model 3566 ac milliohm meter) were also carried out at 1 kHz during all experiments.

Results and Discussion

Prior to cold startup of a PEFC, gas purge is necessary to remove residual water in the cell and thus to create a favorable initial condition to accommodate water produced during cold start. Using the present transparent cell, we observed that a 2 min dry gas purge is sufficient to remove the liquid water from the gas channels, cathode GDL (i.e., silver mesh), and CL surfaces on the cathode. Moreover, the HFR data (not shown here) showed that the membrane resistance increases during gas purge, indicating that the membrane and ionomers in the cathode CL are partially dehydrated by purge gas.

Cold startup from −5°C was performed by feeding dry hydrogen and air and setting the current density at 0.02 A/cm^2. Figure 2a shows a picture of the CCM surface immediately prior to cold start. Figure 2b shows the image when the startup operation was completed (at the cutoff voltage of 0.1 V). The view in Fig. 2 (or Fig. 3, 4, and 6) is of one square in the silver mesh and in the center portion of flowfield. As seen in Fig. 2b, throughout the cold start, no water droplets, frost, or ice can be observed on the surface of CCM. The surfaces of the silver mesh, current collector, and flow channels were also carefully checked using the camera. No water, frost, or ice was found. In this experiment, silver mesh was used as the cathode GDL in place of carbon paper, giving rise to a rather high internal cell resistance (i.e., 1.5 Ω cm^2) at the temperature of −5°C.

To better interpret experimental results, it is instructive to analyze water destination during cold start. The product water (W_{water}, g/cm^2) generated during cold start can be simply calculated from the charge transfer density, namely

$$W_{water} = \frac{it}{2F} M_{H2O} \quad [1]$$

where t is time, i current density, F Faraday's constant, and M_{H2O} the molecular weight of water. Because ice generated in the cathode CL reduces the active Pt area as well as the rate of oxygen transport through the CL, the duration of cold-start operation at −5°C is only 241 s and the amount of product water calculated from Eq. 1 is 0.45 mg/cm^2.

During cold start, a portion of the water produced by ORR in the cathode is removed by reactant gases exiting the cell. The remainder of product water accumulates inside the cell. The amount of water leaving the cell ($m_{water,out}$, g) in the exhaust gas can be estimated by

$$m_{water,out} = \left(N_{H_2} - \frac{iA}{2F}\right) t \frac{p^a_{water}}{p^a - p^a_{water}} M_{H2O} + \left(N_{air} - \frac{iA}{4F}\right) t \frac{p^c_{water}}{p^c - p^c_{water}} M_{H2O} \quad [2]$$

where N_{H2} and N_{air} are the molar flow rates of hydrogen and air

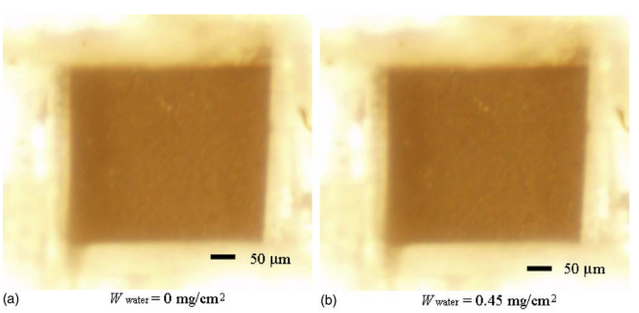

Figure 2. (Color online) Images on the CCM surface during startup from −5°C. (Purge conditions: $T_{purge} = 55$°C, $t_{purge} = 120$ s. Startup conditions: $T_{cell} = -5$°C, $i = 0.02$ A/cm^2, $N_{H2} = N_{air} = 1.487 \times 10^{-5}$ mol/s, $RH_{H2} = RH_{air} = 0\%$, $p_{H2} = p_{air} = 1$ atm.)

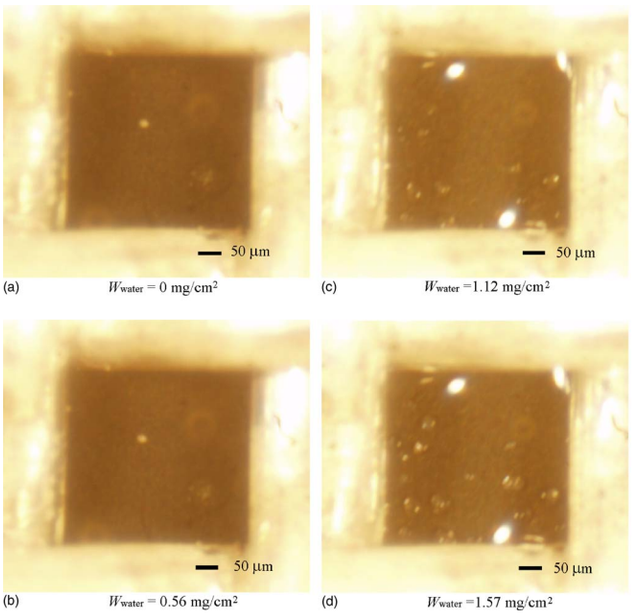

Figure 3. (Color online) Images on the CCM surface during startup from −3 °C. (Purge conditions: T_{purge} = 55 °C, t_{purge} = 120 s. Startup conditions: T_{cell} = −3 °C, i = 0.02 A/cm², $N_{H2} = N_{air}$ = 1.487 × 10^{-5} mol/s, $RH_{H2} = RH_{air}$ = 0%, $p_{H2} = p_{air}$ = 1 atm.)

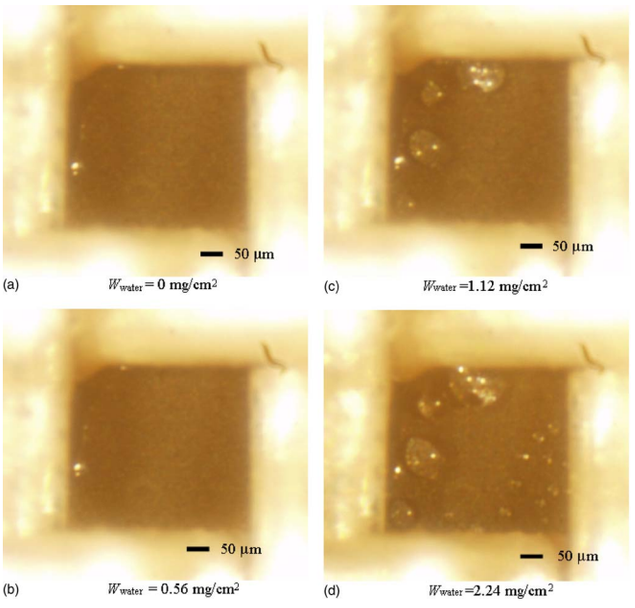

Figure 4. (Color online) Images on the CCM surface during startup from −1 °C. (Purge conditions: T_{purge} = 55 °C, t_{purge} = 120 s. Startup conditions: T_{cell} = −1 °C, i = 0.02 A/cm², $N_{H2} = N_{air}$ = 1.487 × 10^{-5} mol/s, $RH_{H2} = RH_{air}$ = 0%, $p_{H2} = p_{air}$ = 1 atm.)

entering the cell (mol/s), respectively, A the active area of the electrode, p^a and p^c the gas pressures of the anode and cathode (Pa), and p^a_{water} and p^c_{water} the water partial pressures of the anode and cathode. The saturation vapor pressure at −5 °C is equal to 401.76 Pa.[17] If we assume that hydrogen and air leave the cell at the relative humidity of 50 and 100%, respectively, the amount of water exiting the anode and cathode during the cold start (T = −5 °C, p^a_{water} = 200.88 Pa, p^c_{water} = 401.76 Pa, t = 241 s, $N_{H2} = N_{air}$ = 1.487 × 10^{-5} mol/s) is 0.12 and 0.25 mg, respectively. That is, there is 0.08 mg/cm² product water carried away by the exhaust gases. This leaves 0.37 mg/cm² product water in the cell, part of which remains in the cathode CL and part of which has migrated into the membrane.

The water storage capacities of the cathode catalyst layer based on its open pore volume ($W_{cap,CL}$, g/cm²) and the membrane based on its water uptake potential ($W_{cap,m}$, g/cm²) can be estimated as follows

$$W_{cap,CL} = \delta_{CL}\varepsilon\rho_{ice/water} + \delta_{CL}\varepsilon_m c_{f,dry}\Delta\lambda_{av,CL}M_{H2O} \quad [3]$$

$$W_{cap,m} = \delta_m c_{f,dry}\Delta\lambda_{av,m}M_{H2O} \quad [4]$$

where δ_{CL} is the thickness of catalyst layer, ε the CL porosity, ρ_{ice} the ice density, ε_m the volume fraction of ionomers in the CL, $c_{f,dry}$ the fixed charge concentration in dry Nafion ionomers, and $\Delta\lambda_{av,CL}$ and $\Delta\lambda_{av,m}$ the difference in the average water content before and after cold start in the CL and membrane, respectively. Here, λ denotes the number of water molecules per sulfonic acid group in the ionomer. In our experiment of cold start from −5 °C, the membrane water content prior to cold start, after the cell is purged with dry gases at 55 °C for 2 min, is roughly equal to 6 as estimated from the measured HFR and proton conductivity relation from Ju et al.[18] If we assume that the average water content (λ_{av}) in the membrane and ionomers in the cathode CL reaches 14 after cold start, using typical structural and physical parameters of the CL (δ_{CL} = 10 μm, ε = 0.33, ρ_{ice} = 0.918 g/cm³, ε_m = 0.2, and $c_{f,dry}$ = 1.818 × 10^{-3} mol/cm³), the amounts of ice and water that can be stored in the cathode CL are estimated to be 0.36 and 0.38 mg/cm², respectively. Here, use has been made of a lower limit of the CL porosity (i.e., 0.33) by excluding nonconnected or dead pores. Similarly, 0.47 mg/cm² water can be stored in the membrane of 18 μm thickness if the membrane water content is raised from 6 initially to 14 at full hydration. Based on these estimates, the total product water of 0.45 mg/cm² achieved in the −5 °C startup case appears to be lower than that required for water to emerge from the CL. This supports the observation that no water is detected on the CCM surface, as shown in Fig. 2. A comparison of the product water achieved at shutdown (i.e., 0.45 mg/cm²) to the theoretical water storage capacity of the membrane and cathode catalyst layer (i.e., 0.85 mg/cm²) implies that product water does not fully diffuse into and hydrate the entire membrane due to low water diffusivity at the subzero temperature.

Figure 3 shows CCM surface during startup from −3 °C. All other conditions remained the same as in the first experiment. These images show that when the amount of product water was ≤0.56 mg/cm² (from Eq. 1), which occurred at 300 s from the start of the experiment, no ice, frost, or liquid water was observed. However, when the amount of product water reached 1.12 mg/cm², it began to emerge from the CL as liquid droplets. The water droplet diameters were seen to be only 10–40 μm. When the amount of product water increased to 1.57 mg/cm², the cell potential had decreased to 0.1 V and the startup operation was terminated. It was found that water droplets expanded in size with time and new droplets continually appeared on the surface of CCM.

During this cold-start experiment (T = −3 °C, p^a_{water} = 238.03, p^c_{water} = 476.06 Pa, t = 600 s, $N_{H2} = N_{air}$ = 1.487 × 10^{-5} mol/s), the amounts of water exiting the anode and cathode with the exhaust gas, at the product water W_{water} of 1.12 mg/cm², are 0.37 and 0.75 mg, respectively, or 0.22 mg/cm² total. Thus, there is 0.90 mg/cm² of product water remaining in the MEA. As analyzed earlier, the theoretical capacity of water accumulation in the cathode CL and membrane add up to be 0.85 mg/cm². Therefore, it is reasonable that product water begins to emerge on the CCM surface when the amount reaches 1.12 mg/cm², as visually captured by the images.

Figure 3 also indicates that liquid water, in the form of round droplets, appears on the surface of CCM although the land temperature is kept at −3 °C. This implies that the temperature on the CL

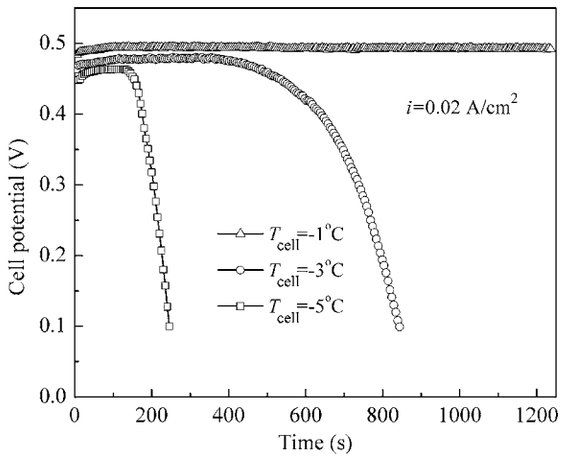

Figure 5. Cell voltage curves for startup from −5°C, −3°C and −1°C. (Purge conditions: T_{purge} = 55°C, t_{purge} = 120 s. Startup conditions: i = 0.02 A/cm^2, $N_{H2} = N_{air}$ = 1.487 × 10^{-5} mol/s, $RH_{H2} = RH_{air}$ = 0%, $p_{H2} = p_{air}$ = 1 atm.)

surface lies above 0°C, possibly due to a temperature difference of 3°C between the land and catalyst layer. This large temperature difference is reasonable because the silver mesh GDL features point contacts with the CL surface and hence there exists a large thermal contact resistance between the silver mesh and catalyst layer. Using the same temperature difference between the land and catalyst layer, one can deduce that the CL surface temperature in the −5°C startup experiment is equal to approximately −2°C. This local temperature, combined with the state of water being ice inside the CL, as inferred from the in situ images in Fig. 2 and 3, suggests that the freezing-point depression of water within the CL may be only 2°C at most. This amount should be negligible in cold-start theory and practice for the startup temperature range between −20 and −30°C of interest for automotive applications. Here, the freezing-point depression, defined as the difference between the freezing point in small pores and the normal equilibrium temperature of water (i.e., 273.15 K), is inversely proportional to the pore radius according to the well-known Gibbs–Thomson relation. That is, the freezing point of water is lowered in confined spaces as the size decreases.

The temperature dependences of the state of water on the surface of the cathode CL and the maximum product water from a cell were further studied by an additional experiment of cold start from −1°C. The corresponding images are shown in Fig. 4. At −1°C, the cell can operate indefinitely. Similar to the −3°C startup case, no water was observed on the surface of CCM when the amount of product water reached 0.56 mg/cm^2. Then, liquid water droplets appeared when the amount of product water became 1.12 mg/cm^2. In this cold-start experiment (T = −1°C, p^a_{water} = 281.34, p^c_{water} = 562.67 Pa, t = 600 s, $N_{H2} = N_{air}$ = 1.487 × 10^{-5} mol/s), the amounts of water carried away from the anode and cathode of the cell by exhaust gases are estimated to be 0.43 and 0.88 mg, respectively, or 0.26 mg/cm^2 total. This leaves 0.86 mg/cm^2 water accumulated in the CCM when the product water reaches 1.12 mg/cm^2. Because the maximum water storage capacity of the cathode CL and membrane together is calculated to be 0.85 mg/cm^2, one expects product water to emerge at this moment. Voltage curves for all three cold-start experiments are compared in Fig. 5.

To summarize, the in situ images of water behavior on the CL surface show that at −5°C, the CL surface could be at ~−2°C and product water inside the CL is ice, which plugs the open pores of the CL and shuts down cell operation. The achievable product water is only 0.45 mg/cm^2, insufficient to emerge onto the CL surface and thus to be observed. At startup temperatures of −3 and −1°C, however, the CL surface temperature is already above the freezing point;

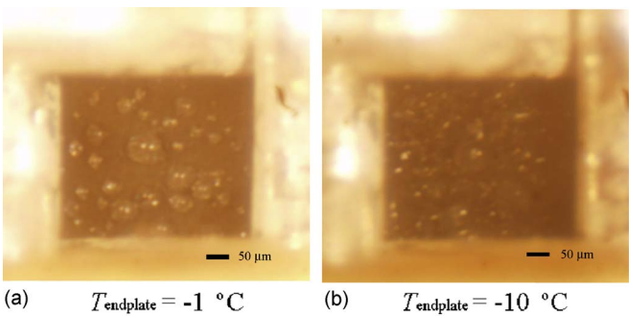

Figure 6. (Color online) Phase transition from water droplets to ice particles. Water droplets are generated during cold start from −1°C and observed on the CCM surface. When the cell is cooled to −10°C for 150 min, water droplets become ice particles.

as such, the product water from ORR is transported out of the CL as liquid and vapor. Water droplets are clearly observed and the achievable product water is substantially larger.

One way to distinguish water droplets from ice/frost particles on the CCM surface during visualization experiments is the fact that droplets are clearly growing if viewed from a movie file (not shown here). To further confirm that what was observed on the surface of CCM as shown in Fig. 3c, 3d, 4c, and d is liquid water but not ice or frost, a "quenching" experiment followed immediately after the cold start at −1°C by turning off the current load, shutting off the inlet and outlet gases, and cooling down the cell rapidly using a coolant bath. In this process, the liquid water on the CCM surface underwent phase transition from liquid to ice or frost on the CL surface, as shown in Fig. 6. Figure 6a displays the water droplets generated during cold start at −1°C. When the cell temperature was lowered to −10°C and maintained there for 150 min, long enough to make the CL surface temperature drop below 0°C, ice was found on the CCM surface, as shown in Fig. 6b. Ice particles thus formed are very small (~10 μm diam), as measured with the high-magnification camera. Further, water droplets and ice particles on the CCM surface differ in shape; the water droplets appear round, while the ice particles are irregular. Another quenching experiment was carried out after cold startup from −3°C by maintaining cell temperature at −3°C for 2 h. Water droplets on the CCM surface also turned to ice particles at −3°C when there was no electrochemical reaction and thus no heat generated inside the cell. This second quenching experiment further confirms that the freezing-point depression in the CL is quite small and its influence on the cold start behavior should be negligible.

Another interesting experiment was carried out to observe water transport from the CL surface to the hydrophilic surface of the mesh wires after ice melting and during cell warm-up. At the end of the

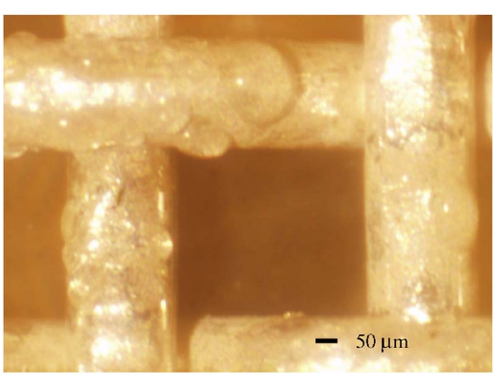

Figure 7. (Color online) Water transport from the CCM surface to the hydrophilic surface of silver wires during ice melting and cell warm-up.

quenching experiment to −10°C as described above, gas flows to and from the cell and the current were stopped. The cell temperature was allowed to rise to room temperature (~25°C) where it remained for 15 h. It was seen that ice particles on the CL surface melted when its temperature became higher than the freezing point, and the resulting liquid water was wicked onto the more hydrophilic mesh wires, as shown in Fig. 7. This liquid water movement after ice melting (and presumably also before cooling down to a subfreezing temperature) underscores the effectiveness of using highly hydrophilic components to drain liquid water from the CL and thus to create a more favorable condition to store product water generated during cold start.

While the use of silver mesh as the cathode GDL enables optical access to the CL surface, excessive thermal and electric contact resistances existing between the mesh and CL surface disturb a realistic fuel cell operation and prevent the cell from drawing high current densities. Thus, better visualization techniques that provide both realistic fuel cell environment and optical access to the catalyst layer should be pursued in future research.

Conclusion

A transparent fuel cell using silver mesh as the cathode GDL has been employed to visually study liquid water and ice formation during PEFC cold start. At startup temperature of −5°C and current density of 0.02 A/cm^2, the achievable product water is only 0.45 mg/cm^2, which is insufficient to emerge on the CL surface. The product water from ORR most likely exists in the catalyst layer as ice in this case. At startup temperatures of −3 and −1°C, the product water is seen to transport out of the CL in the form of liquid droplets of ~10 μm in diameter, indicating no ice formation inside the CL surface. Therefore, the freezing-point depression of water in the CL is only 2°C at most, and its influence on cold-start behavior should be negligible. This visualization study also reveals the possibility of liquid water transport from the CL surface to more hydrophilic mesh wires under capillary wicking. This wicking mechanism may prove useful to remove liquid water from the catalyst layer by using an adjacent hydrophilic component during cell cool-down and warm-up. Work is ongoing to further probe ice formation inside the catalyst layer during PEFC startup from very low temperatures, a topic of special interest for automotive applications.

Acknowledgments

Financial support of this work by Nissan Motor Co. Ltd. is gratefully acknowledged. The authors also thank Dr. Richard Steinberger for the help in design of the imaging system and assistance in carrying out experiments, as well as Y. Tabuchi and Dr. K. Yoshizawa of Nissan and Kazuya Tajiri and Leng Mao of ECEC for many useful discussions.

The Pennsylvania State University assisted in meeting the publication costs of this article.

References

1. M. S. Wilson, J. A. Valerio, and S. Gottesfeld, *Electrochim. Acta*, **40**, 355 (1995).
2. E. A. Cho, J. J. Ko, H. Y. Ha, S. A. Hong, K. Y. Lee, T. W. Lim, and I. H. Oh, *J. Electrochem. Soc.*, **150**, A1667 (2003).
3. E. A. Cho, J. J. Ko, H. Y. Ha, S. A. Hong, K. Y. Lee, T. W. Lim, and I. H. Oh, *J. Electrochem. Soc.*, **151**, A661 (2004).
4. R. C. McDonald, C. K. Mittelsteadt, and E. L. Thompson, *Fuel Cells*, **4**, 208 (2004).
5. J. St-Pierre, J. Roberts, K. Colbow, S. Campbell, and A. Nelson, *J. New Mater. Electrochem. Syst.*, **8**, 163 (2005).
6. F. Kagami, Y. Hishinuma, and T. Chikahisa, *Therm. Sci. Eng.*, **10**, 25 (2002).
7. Y. Hishinuma, T. Chikahisa, F. Kagami, and T. Ogawa, *JSME Int. J., Ser. B*, **47**, 235 (2004).
8. M. Oszcipok, D. Riemann, U. Kronenwett, M. Kreideweis, and M. Zedda, *J. Power Sources*, **145**, 407 (2005).
9. M. Cappadonia, J. W. Erning, S. M. S. Niaki, and U. Stimming, *Solid State Ionics*, **77**, 65 (1995).
10. M. Cappadonia, J. W. Erning, and U. Stimming, *J. Electroanal. Chem.*, **376**, 189 (1994).
11. M. Saito, K. Hayamizu, and T. Okada, *J. Phys. Chem. B*, **109**, 3112 (2005).
12. D. Chu, R. Jiang, K. Gardner, R. Jacobs, J. Schmidt, T. Quakenbush, and J. Stephens, *J. Power Sources*, **96**, 174 (2001).
13. R. K. Ahluwalia and X. Wang, *J. Power Sources*, **139**, 152 (2005).
14. B. K. Datta, G. Velayutham, and A. P. Goud, *J. Power Sources*, **106**, 370 (2002).
15. X. G. Yang, F. Y. Zhang, A. L. Lubawy, and C. Y. Wang, *Electrochem. Solid-State Lett.*, **7**, A408 (2004).
16. F. Y. Zhang, X. G. Yang, and C. Y. Wang, *J. Electrochem. Soc.*, **153**, A225 (2006).
17. *CRC Handbook of Chemistry and Physics*, 77th ed., D. R. Lide, Editor, CRC Press, Boca Raton, FL (1997).
18. H. Ju, C. Y. Wang, S. Cleghorn, and U. Beuscher, *J. Electrochem. Soc.*, **152**, A1645 (2005).